Applied Catalysis B: Environmental 235 (2018) 75–83

Contents lists available at ScienceDirect

Applied Catalysis B: Environmental

journal homepage: www.elsevier.com/locate/apcatb

Fe and Cu in humic acid extracts modify bacterial inactivation pathways during solar disinfection and photo-Fenton processes in water

Jazmin Porras[a,b,c], Stefanos Giannakis[c], Ricardo A. Torres-Palma[d,*], Jhon J. Fernandez[a], Michaël Bensimon[e], Cesar Pulgarin[c,*]

[a] Química de Recursos Energéticos y Medio Ambiente (QUIREMA), 2 Grupo de Investigación en Remediación Ambiental y Biocatálisis (GIRAB), Instituto de Química, Facultad de Ciencias Exactas y Naturales, Universidad de Antioquia UdeA, Calle 70 No. 52-21, Medellín, Colombia
[b] Grupo de Investigaciones Biomédicas Uniremington, Facultad de Ciencias de la Salud, Corporación Universitaria Remington (Uniremington), Calle 51 No. 51-27, Medellín, Colombia
[c] School of Basic Sciences (SB), Institute of Chemical Science and Engineering (ISIC), Group of Advanced Oxidation Processes (GPAO), École Polytechnique Fédérale de Lausanne (EPFL), Station 6, CH-1015, Lausanne, Switzerland
[d] Grupo de Investigación en Remediación Ambiental y Biocatálisis (GIRAB), Instituto de Química, Facultad de Ciencias Exactas y Naturales, Universidad de Antioquia (UdeA), Calle 70 No. 52-21, Medellín, Colombia
[e] School of Architecture, Civil and Environmental Engineering (ENAC), Environmental Engineering Institute (IIE), Central Environmental Laboratory (CEL), Ecole Polytechnique Fédérale de Lausanne (EPFL), Station 18, 1015, Lausanne, Switzerland

ARTICLE INFO

Keywords:
SODIS
Triplet states
Organic matter
Disinfection
Metal
Water treatment

ABSTRACT

The literature suggests a dual role for humic acids involving both agonistic and antagonistic processes in the photo-chemical cycle in water. In this work, the use of Fe- and Cu-containing humic acid (HA) extracted from coal waste was evaluated for the enhancement of solar-based disinfection processes, namely solar light (*hv*), *hv*/H_2O_2, and *hv*/H_2O_2/Fe^{2+} (photo-Fenton) processes. The differences in the enhancement of each process are reported herein. The degree of bacterial inactivation during solar disinfection under solar and visible light in the presence of the HAs was negatively correlated with the presence of metals, and was attributed to ^{3}DOM* and $^1O_2$-mediated events. However, the presence of metals greatly enhanced disinfection when H_2O_2 was added by inducing a photo-Fenton process, and significantly reduced the inactivation times (> 50%) due to homogeneous Fe- (Fenton) and Cu-based (Fenton-like)-assisted inactivation pathways. The addition of small quantities of Fe to HA-containing samples further enhanced the inactivation due to the ample generation of highly photo-active Fe-HA complexes. The result was a further ~60% reduction in exposure time to achieve a 7-log bacterial reduction, as well as the degradation of the HA itself as a sacrificial electron donor, via an Fe-mediated ligand to metal charge transfer process. This work reveals new pathways in disinfection assisted by metal-containing HAs, and demonstrates their efficiency in reducing microbial loads with simultaneous elimination of the additive.

1. Introduction

Solar disinfection of drinking water (SODIS) is a well-established process for water sterilization in developing countries [1]. Despite the relative success of this process, its limitations, namely its requirement for low turbidity, low treatment volumes (up to 2 L), temperature dependence, and the risk of microbial regrowth during storage after treatment [2], have prompted an array of works on its enhancement. One of the most promising improvements is the photo-Fenton process. This method not only builds upon the base process (the use of solar light) [3], but also takes advantage the ubiquitous presence of iron and the photo-generation of hydrogen peroxide to produce the highly oxidative hydroxyl radical [4], which can readily and effectively inactivate the majority of microorganisms. The addition of Fe and H_2O_2 enhances the overall efficiency of the system, but the elucidation of the exact inactivation pathways is far from a simple process; when near-neutral (natural) water is involved, the presence of inorganic substances, such as carbonate and sulfate, and organic substances, such as natural organic matter (NOM) [5] induce further pathways, for which information is scarce.

Abbreviations: CDOM, chromophoric DOM; DOM, dissolved organic matter; EDS, energy dispersive X-ray spectroscopy; HA, humic acid; HA_{MC}, humic $acid_{mineral\ content}$; HS, humic substances; hv, acronym for "light"; ICP-MS, inductively coupled plasma mass spectrometry; LMCT, ligand-to-metal charge transfer; NOM, natural organic matter; ROS, reactive oxygen species; SEM, scanning electron microscopy; SODIS, solar disinfection

* Corresponding authors.
E-mail addresses: ricardo.torres@udea.edu.co (R.A. Torres-Palma), cesar.pulgarin@epfl.ch (C. Pulgarin).

https://doi.org/10.1016/j.apcatb.2018.04.062
Received 6 March 2018; Received in revised form 21 April 2018; Accepted 25 April 2018
Available online 30 April 2018
0926-3373/

Humic substances (HS) comprise the majority of dissolved organic matter (DOM) in aquatic systems. HS may also be considered the main precursor of excited triplet states (exogenous photosensitizers), which are able to degrade organic compounds and inactivate microorganisms such as bacteria and viruses [6–11]. Humic acids absorb light in the UVA and visible spectrum to form excited states that can attack biomolecules or react with oxygen to generate reactive oxygen species (ROS). More specifically, under UV–vis irradiation and in the presence of O_2, the substances can produce ROS such as singlet oxygen ($^1O_2$) and superoxides (HO_2/O_2^-) (Eqs. (1)–(4)) [12–14].

$$HA + h\nu \rightarrow {}^1HA^* \quad (1)$$

$$^1HA^* \rightarrow {}^3HA^* \quad (2)$$

$$^3HA^* + O_2 \rightarrow HA^* + {}^1O_2 \quad (3)$$

$$^3HA^* + O_2 \rightarrow HA^{\bullet+} + O_2^{\bullet-} \quad (4)$$

The literature describes the different roles of organic matter in photosensitization events, which depending on the type of functional groups present in the HS. For instance, ketonic [15,16] and quinonic groups [17,18] have been shown to be the most photo-chemically active. Various methods, including spectroscopic and fluorescence methods, have been used to characterize the organic matter and predict or correlate its photo-activity with specific characteristics [19–22]. Additionally, the quantity of HAs present also plays an important role in the net outcome; in addition to its action as a light screen [23,24], Porras et al. investigated the photo-transformation of drugs and pesticides using different humic substances in different quantities, and showed a correlation between the structural characteristics of the humic substances and their photo-transformation activity. An antagonistic effect was noted at high HA concentrations, indicative of light attenuation or self-inhibition [25,26].

The organic substances present in natural water can also affect solar-based treatment processes, including SODIS [27,28], photo-catalysis [29,30], and photo-Fenton [31,32] processes. For instance, Giannakis et al. described both the beneficial action of HAs in maintaining a homogeneous photo-Fenton reaction [33] and the implications when a heterogeneous mode was employed for the inactivation of viruses [34]. The organic matter could enhance or inhibit photo-assisted disinfection processes, regardless of the target microorganism [3]. In all the aforementioned studies, pure NOM isolates or model NOM compounds were used. Their ability to complex iron is the source of the enhanced activity (Eq. (5)) [35,36], but the literature lacks studies of naturally metal- and mineral-bearing humic substances and their effects on solar-related disinfection processes, in which they could initiate Fenton (Fe-based) and Fenton-like (Cu-based reactions) as follows (Eqs. (6)–(19)):

$$(Fe^{3+} - HA) + h\nu \rightarrow Fe^{2+} + HA_{ox}^{+} \quad (5)$$

Fenton

$$Fe^{2+} + H_2O_2 \rightarrow Fe^{3+} + HO^{\bullet} + OH^- \quad (6)$$

$$Fe^{3+} + H_2O_2 \leftrightarrow (Fe^{3+}(HO_2))^{2+} + H^+ \quad (7)$$

$$Fe^{3+} + H_2O \leftrightarrow Fe(OH)^{2+} + H^+ \quad (8)$$

$$(Fe^{3+}(OH)(HO_2))^{+} \rightarrow Fe^{2+} + HO_2^{\bullet} + OH^- \quad (9)$$

$$Fe^{2+} + HO^{\bullet} \rightarrow Fe^{3+} + OH^- \quad (10)$$

$$Fe^{2+} + HO_2^{\bullet} \rightarrow (Fe^{3+}(HO_2))^{2+} \quad (11)$$

$$Fe^{2+} + O_2^{\bullet-} + H^+ \rightarrow (Fe^{3+}(HO_2))^{2+} \quad (12)$$

$$Fe^{3+} + HO_2^{\bullet} \rightarrow Fe^{2+} + O_2 + H^+ \quad (13)$$

$$Fe^{3+} + O_2^{\bullet-} \rightarrow Fe^{2+} + O_2 \quad (14)$$

Fenton-like

$$Cu^{+} + H_2O_2 \rightarrow Cu^{2+} + HO^{\bullet} + HO^- \quad (15)$$

$$Cu^{2+} + H_2O_2 \rightarrow Cu^{+} + O_2^{\bullet-} + 2H^+ \quad (16)$$

$$Cu^{+} + O_2 \rightarrow Cu^{2+} + O_2^{\bullet-} \quad (17)$$

$$Cu^{+} + O_2^{\bullet-} \xrightarrow{2H^+} Cu^{2+} + H_2O_2 \quad (18)$$

$$Cu^{2+} + O_2^{\bullet-} \rightarrow Cu^{+} + O_2 \quad (19)$$

The aim of this research was to study the role of HA, as a model of DOM, on bacterial disinfection in several solar-based processes. The presence of metals (i.e., Fe and Cu) and their photo-chemical implications were investigated. After characterization of the HA samples, their effects on SODIS (*hν*), *hν*/H_2O_2, and *hν*/H_2O_2/Fe (photo-Fenton) processes were considered. Special attention has been given to the use of solar light alone, as it is the process on which the other two are based. The complex photo-Fenton process has been broken down into its constituent steps, and the use of HAs that inherently contain metals have been assessed. A detailed disinfection and spectroscopic study to investigate the variables involved, namely the quantity (initial concentration) and composition of the HS, was attempted using three HAs (HA_1, HA_5, and HA_{16}) containing different amounts of mineral matter (1, 5, and 16%, respectively). The results indicate the pitfalls and opportunities for enhancement of the photo-chemical disinfection of water when HAs are naturally present or intentionally added.

2. Materials and methods

2.1. Chemicals and reagents

All chemicals were of reagent grade. Hydrogen peroxide 30% and iron (II) sulfate heptahydrate ($FeSO_4{\cdot}7H_2O$) were provided by Merck. Titanium (IV) oxysulfate ($TiOSO_4$) for the spectrophotometric determination of H_2O_2 was provided by Fluka. All solutions were prepared with Milli-Q water (18.2 MΩ cm) immediately prior to irradiation. Reagent grade NaOH, HCl, and HF were provided by Sigma-Aldrich.

2.2. Preparation of humic acid (HA) fractions

The terrestrial humic acid sample referred to as HA_{MC} (humic acid mineral content) was obtained from an air-modified low-rank coal mine in the Amaga region in Colombia and extracted in the laboratory as reported previously [25]. The obtained HA_{MC} fraction was washed with deionized water and finally freeze-dried; this sample was labeled as HA_{16} (based on its mineral matter content percentage). A given quantity of HA_{16} was demineralized by stirring in a 0.1:0.3M solution of HCl:HF for 36 h at room temperature under a nitrogen atmosphere. This demineralized humic acid fraction was washed with deionized water and freeze-dried; the resulting sample was labeled as HA_5. Finally, a portion of the HA_5 was demineralized using the same procedure to yield the sample labeled as HA_1. Thermogravimetric analysis of the humic acids HA_{16}, HA_5 and HA_1 was carried out with a TA-Instruments Q500 using air at 900 °C, and the samples produced 16, 5, and 1% of mineral-containing ash, respectively.

The morphology and elemental composition of the ash samples were determined using scanning electron microscopy (SEM) with a JEOL JSM 6490 instrument with a LaB_6 filament and equipped with an energy dispersive X-ray spectroscopy (EDS) analyzer at a 20 kV accelerating voltage. The powder samples were sputter coated with gold using a Sputter Coater SC502 prior to analysis. The backscattered electron (BSE) detection mode was used. Finally, elemental analysis was performed using a LECO Truspec analyzer. 2 mg of the solid sample was combusted, and compositional analysis of the total gas was carried out by selective thermal conductivity (TCD) cells and infrared (IR).

2.3. Analytical methods

The evolution of the H_2O_2 concentration was measured using a colorimetric method based on the absorbance of the yellow complex formed between titanium (IV) oxysulfate and H_2O_2 at 410 nm using a spectrophotometer (Perkin-Elmer UV–vis lambda 20 Spectrophotometer). To determine the H_2O_2 concentration, a calibration curve of six points from 0 to 20 mg/L H_2O_2 was used ($R^2 > 0.99$). The pH (pH/Ion S220, Seven Compact, Mettler Toledo) of the samples was measured before and after each treatment. Elemental analysis of the samples was carried out by the conventional combustion method using a Perkin–Elmer CHN-O analyzer. Finally, iron and copper measurements were conducted using ICP-MS as in [33].

2.4. Photochemical indices

The ratios E_2/E_3 and E_4/E_6 were calculated using the absorption coefficients at 254, 364, 465, and 565 nm. $SUVA_{254}$ is defined as the absorption coefficient at 254 nm divided by the measured DOC concentration in milligrams per liter (mg/L). ε_{280} is the optical density at 280 nm, which is defined as the absorption coefficient at 280 nm divided by the measured DOC concentration in milligrams per liter. The spectral slopes measured at 275–290 and 350–450 nm and the slope ratio (S_R: Slope 275–290/Slope 350–450) were obtained by plotting the natural logarithm of the absorption coefficient (a/m^{-1}) against the wavelength (λ/nm). The value of the absorption coefficient was obtained from Eq. (20).

$$a = \frac{2.303*A}{l} \quad (20)$$

where A is the absorbance and l (m) is the length of the absorption cell.

2.5. Bacterial strain and growth media

The bacterial strain used was *E. coli* K12 and was supplied by DSM (No. 498), German Collection of Microorganisms and Cell Cultures. *E. coli* K12 is non-pathogenic and approximates wild-type *E. coli*, a typical indicator bacterium for enteric pathogens. Strain samples were stored in cryo-vials containing 20% glycerol at 20 °C. Bacterial pre-cultures were prepared for each series of experiments by streaking a colony from the strain sample onto plate count agar (PCA, Merck). Subsequently, the plates were incubated for 24 h at 37 °C in a Heraeus incubator. One of the growing colonies was re-plated on a separate PCA and incubated again for 24 h at 37 °C.

To prepare the bacterial pellet for the experiments, one colony was picked from among the pre-cultures and loop-inoculated into a 50 mL sterile PE Eppendorf flask containing 5 mL of Luria-Bertani (LB) medium. The flask was then incubated at 37 °C and 180 rpm in a shaker incubator. After 8 h, the cells were diluted (1% v/v) in a 500 mL Erlenmeyer flask containing 150 mL of pre-heated LB broth and incubated aerobically at 37 °C for 16 h until a stationary physiological phase was reached. The bacterial growth and the stationary phase were monitored by optical density at 600 nm. The LB medium consisted of sodium chloride (10 g), tryptone (10 g), and yeast extract (5 g) in 1 L of deionized water; this solution was then sterilized by autoclaving for 20 min at 121 °C.

The cells were harvested by centrifugation (15 min at 5000 × *g* and 4 °C) in a universal centrifuge (Hermle Z323K). The bacterial pellet was re-suspended and washed three times with a saline solution (NaCl/KCl). The final pellet was re-suspended in saline solution to the initial volume. This procedure resulted in a cell density of approximately 10^9 colony forming units (CFU) per milliliter. The bacterial solution was diluted in the water samples used in the experiments to a cell density corresponding to 10^7 CFU mL^{-1}. The saline solution was composed of sodium chloride (8 g) and potassium chloride (0.8 g) in 1 L of deionized water. The pH of the solution was adjusted to 7–7.5 and the solution was then sterilized by autoclaving for 20 min at 121 °C.

The bacterial concentration in the samples (in CFU/mL) was determined by plating on a non-selective cultivation media, plate count agar (PCA). 1 mL of the sample was withdrawn during the experiments, and was immediately plated using the standard plate count method. The plates were incubated for 24 h at 37 °C and the CFU on the plates were counted manually. For each kinetics curve, experiments were repeated at least twice (biological replicates), while sampling and plating was conducted in duplicate (statistical replicates). Furthermore, plating was performed by spreading 0.1 mL of the sample. In order to achieve good distribution (desired concentration: 15–150 colonies per plate), serial dilutions were used for each sample. The data points presented are the average of the biological and statistical replicates, and the error bars indicate the standard deviation from the mean. The aforementioned methodology has successfully been applied in the microbiological testing of natural water, photocatalytic processes, and other microorganisms with low error [62–65].

2.6. Experimental: light source, boundary conditions, and reactors

The samples were placed on a magnetic stirrer in a solar simulator (CPC Suntest Atlas) and 50 mL of sample was irradiated. The NXe lamp (Atlas) had a spectral wavelength distribution with about 0.5% of the emitted photons at wavelengths in the 290–320 nm range (UV-B range) and about 5% from 300 to 400 nm. The emission spectrum of the Suntest mirrors that of the solar spectrum between 400 and 800 nm, and wavelengths shorter than 290 nm are cut off with a filter (see Supplementary Fig. S14). The temperature in the reactor never exceeded 35 °C. The global irradiance was ~600 W/m^2 and UV radiation was ~30 W/m^2, as monitored by a combination of a UV radiometer and a pyranometer connected to a data-logger (CUV and CM6b, respectively, Kipp & Zonen, Defft, Holland). All the experiments were carried out in equilibrium with the air under 350 rpm of agitation. Pyrex reactors of 100 mL were used for all tests, and were autoclaved and acid-washed prior to the experiments.

Different experimental conditions were evaluated using three types of humic acid at near-neutral pH. For all experiments, the initial concentration of bacteria in the water was ≈10^7 CFU/mL. The bacterial cells were dispersed in the water, and the solution was stirred for 20 min in order to provide sufficient time for bacterial acclimatization before starting the experiment. The addition of the reagents (ferrous sulfate and/or hydrogen peroxide) was conducted in a single dosage and the light source was turned on immediately to start the test. Dark control experiments were carried out, and for reproducibility each experiment was carried out in triplicate.

In the experiments without HA, the sample was prepared using Milli-Q water. The experiments with HA were conducted using different concentrations of HA. The concentration of H_2O_2 was dependent on the test, i.e., 10, 15, or 20 mg/L. In the photo-Fenton experiments, the concentrations of the Fe^{2+} and H_2O_2 solutions were 1 mg/L and 20 mg/L, respectively. The pH was adjusted to 6.5–7 by the addition of a 0.1M sodium hydroxide solution.

3. Results and discussion

3.1. Characterization of the humic acid extracts (HA_{MC})

In this study, three humic acid samples with different mineral contents were evaluated. The samples HA_1, HA_5, and HA_{16} contained humic acids extracted from a carbonaceous material, and had mineral matter contents of 1, 5, and 16%, respectively. Fig. 1 shows the SEM results for HA_{16} and HA_5 and demonstrates the surface topography of the samples. The differences between the two samples and their metal contents are clearly indicated by the bright spots in Fig. 1; it is evident that the HA_{16} sample had a higher metal content than HA_5. The qualitative composition was determined using EDS spectra obtained from

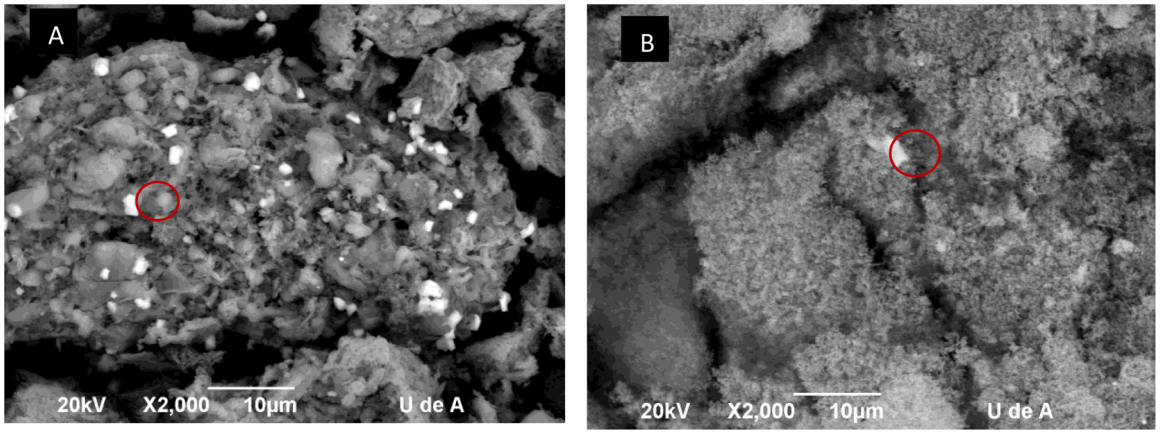

Fig. 1. Scanning electron microscopy (SEM) for the ash of the humic acids used in the study. A) Ash of humic acid with 16% of mineral matter and B) ash of humic acid with 5% of mineral matter.

the red-circled areas in Fig. 1. Table S1 of the supplementary material shows the complete composition of these humic acid ash samples. Among the detected substances, we discuss herein those with the greatest photochemical significance. HA_{16} contained 29.49% of iron and 10.58% of copper minerals, while, as expected, HA_5 presented smaller quantities of these metals, 11.3% and 1.35% for iron and copper, respectively. Finally, as HA_1 was produced by further demineralization of HA_5 and contained only 1% mineral matter, this analysis was not carried out, and it can be safely assumed that its mineral content was negligible.

3.2. Effect of Fe and Cu-bearing humic acids on bacterial inactivation by solar light (hv)

3.2.1. Effect of HA concentration on solar disinfection

In order to estimate the effect of the HA concentration on solar disinfection, HA_1 was used to minimize interference and possible extra catalytic events due to mineral content. The inactivation of *E. coli* by solar light in the absence and presence of different concentrations of humic acid (HA_1) is shown in Fig. 2. In the dark, the bacterial concentration remained stable over the 5 h blank test, indicating that the bacteria were not adsorbed into the humic acids, and conversely, that the HA had no inhibitory effect on their viability. The action of sunlight on *E. coli* induced a concentration decrease of 1.2 logU, following the typical shoulder/log-linear kinetic shape [37]. The ability of direct light to cause DNA damage and internal oxidative damage to proteins and other targets in bacteria has been described elsewhere [5]. The addition of 0.5 mg/L humic acid accelerated the inactivation of *E. coli*, increasing the disinfection by between 2 and 3 logU. Additionally, this increase was consistent when the concentration was further increased from 0.5 to 1 mg/L.

However, the positive effect of HA was less pronounced at a HA_1 concentration of 3 mg/L, suggesting that at high concentrations, HA can filter out the light, thus demonstrating a detrimental effect on bacterial disinfection. This filter effect has previously been reported during the evaluation of the effect of HS on the photochemical degradation of chlorotalonil and of a mixture of emerging contaminants, respectively [25,38]. Humic substances can act as photosensitizing substances, but can also act as (self)scavengers. Thus, their role in photochemical reactions is highly dependent on their concentration in the solution.

Furthermore, the formation of singlet oxygen by HA was also demonstrated, with the apparent quantum yield of singlet oxygen production by HA_{16} (Φ_{SO}) being $1.4 \pm 0.2 \times 10^{-2}$ [25]. Singlet oxygen can damage membranes or diffuse into cells, where it can come into contact with DNA, causing strand breaks or nucleic base modifications [39]. Additionally, the addition of light and the excitation of HA to the triplet state can induce further inactivation pathways, such as electron transfer to the bacterial membrane, which leads to membrane destabilization with subsequent bacterial inactivation.

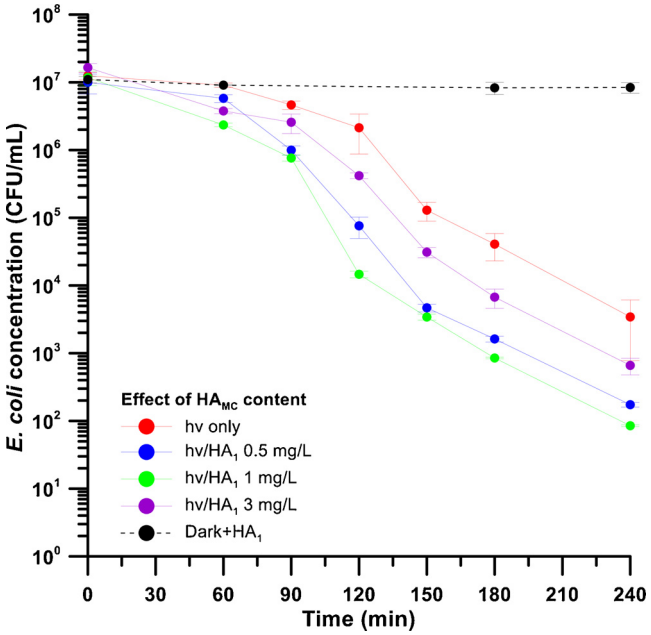

Fig. 2. Inactivation of *E. coli* by solar light (●) in Milli-Q water using different quantities of HA_1 (humic acid with 1% of mineral matter); 0.5 mg/L (●),1 mg/L (●) and 3 mg/L (●) and dark control with 0.5 mg/L HA_1 (●).

In order to determine the contributions from the dominant pathways, i.e., the contributions of $^3HA^*$ and $^1O_2$, the inactivation of *E. coli* was carried out in the absence and presence of HA, using D_2O to increase the lifetime of singlet oxygen ($^1O_2$) in water (Fig. 3). The quenching rate constant of $^1O_2$ by D_2O is approximately 13 times lower than that of H_2O [40]; hence, any difference in inactivation will be attributed to $^1O_2$ and will confirm its generation (or absence) and importance. When D_2O was introduced, the dark controls indicated an insignificant loss of bacterial cultivability (10% of the population), but under light the inactivation was evidently improved in both the presence and absence of HA. These results clearly indicated that the inactivation of *E. coli* inactivation was significantly enhanced in the presence of HA and D_2O.

Since a notable change in kinetics occurred in the presence of D_2O, we can assert that $^1O_2$ is an important factor in HA-mediated inactivation by our isolates. The apparent 1st order inactivation rate constants of the inactivation were calculated for the experiments using solar in MilliQ

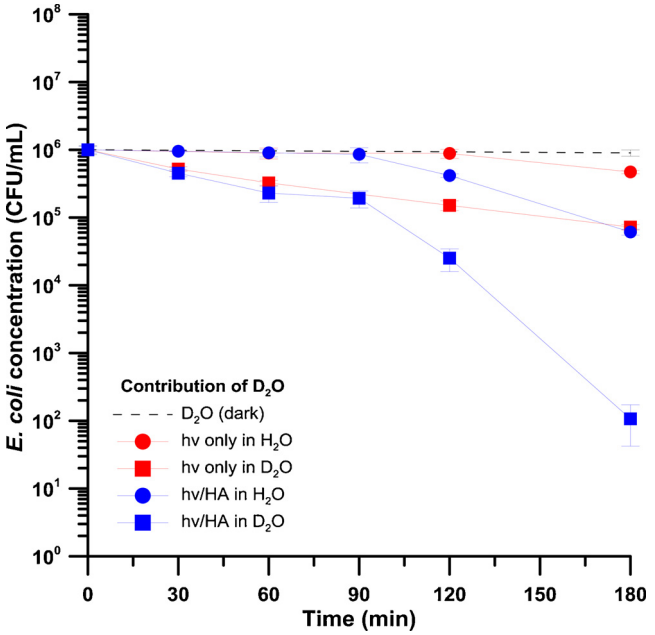

Fig. 3. Inactivation of *E. coli* by solar light (●) in Milli-Q water and 50% D_2O (■) in presence (●) and absence of HA_5 (1 mg/L) (■).

($k_{solar} = 3.8 \times 10^{-3}\,min^{-1}$); solar in 50% D_2O ($k_{solar+D2O} = 0.01\,min^{-1}$); solar + HA_5 in MilliQ ($k_{HA} = 0.04\,min^{-1}$); and solar + HA_5 in 50% D_2O ($k_{HA+D2O} = 0.09\,min^{-1}$). Thus, the kinetics constants followed the order $k_{solar} < k_{solar+D2O} < k_{HA} < k_{HA+D2O}$. The constant k_{HA+D2O} was 9 times greater than that of $k_{solar+D2O}$, indicating the formation of singlet oxygen under irradiation in the presence of HA. In light of these results, we can suggest that this type of humic acids produces singlet oxygen, albeit possibly at lower rates than other non-metal-containing HAs [62]. On the other hand, a relationship between the structural characteristics of humic substances and their photosensitization capacity has been reported [25]. Thus, since HA_5 was used in the transient species investigation, the effect of mineral matter content is evaluated in the next section.

3.2.2. Effect of mineral matter content in solar disinfection

With the main purpose of investigating the effect of the mineral matter content of the humic acids on the inactivation of *E. coli*, experiments using humic acids containing 1, 5, and 16% mineral matter were carried out. Fig. 4A shows that the inactivation in the dark was negligible in all cases. Under solar light, the presence of the humic acids HA_{16}, HA_5 and HA_1 increased the *E. coli* inactivation by 1-logU, 1.1-logU and 2.3-logU after 150 min of treatment. A relationship between the mineral matter content of the humic acids and the inactivation of *E. coli* was observed, with HA_1 showing a higher sensitization effect, followed by HA_5 and HA_{16}. Previous findings suggest that the decreased inactivation by HA_5 and HA_{16} may be due to following factors: (i) A decrease in the transmittance of light in the water due to the minerals present in these humic substances and/or (ii) the higher organic matter content of HA_1 compared to its 5 and 16% counterparts. Taking into account the results in Fig. 2, the latter explanation is most likely.

The simulated solar light tests were followed by identical tests using visible light only in order to investigate the contribution of the chromophoric organic matter. *E. coli* inactivation was carried out using a filter that blocks UVB and UVA light (permitted $\lambda > 400$ nm) in the presence of the same humic acids. In this way, the damage caused to *E. coli* by UVB and UVA would be minimized, and the photo-inactivation would be due mostly to the ROS produced by the chromophoric part of the humic acids used in this investigation. Fig. 4B shows that without the UV contribution and in absence of HA, the inactivation after

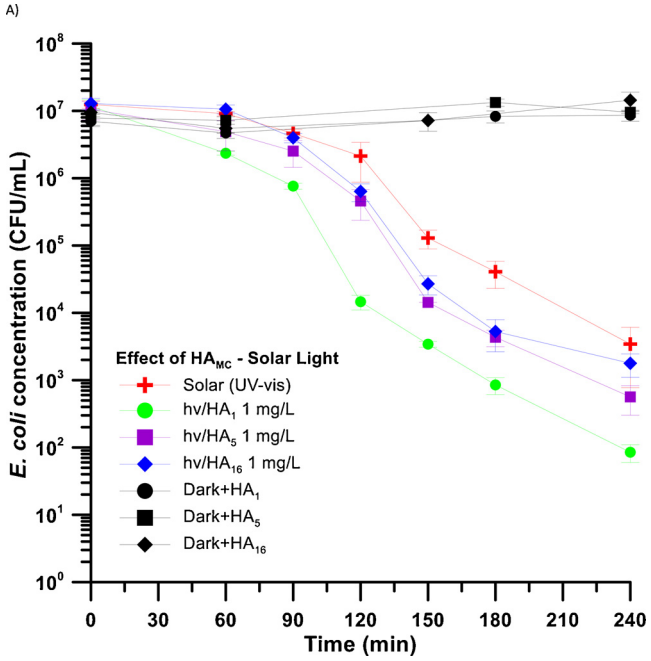

Fig. 4. Photo-inactivation of an *E. coli* suspension in Milli-Q water (pH 6–6.5) containing 1 mg/L of humic acids. (✚) without HA; (●) HA_1; (■) HA_5; (◆) HA_{16} and the dark controls: (-●-)HA_1; (-■-) HA_5; and (-◆-) HA_{16}. A) Under UV–vis light > 290 nm (simulated solar light) and B) using visible light, $\lambda > 400$ nm. Inset: Cut-off filter transmittance.

180 min was negligible. On the other hand, in presence of the humic acids HA_1, HA_5, and HA_{16}, complete inactivation was obtained at 300 min when UVA/UVB light was not permitted. These results indicate that irradiation with visible light in presence of humic substances also generates reactive species that can cause bacterial inactivation, but their inactivation capacity is lower than that of HA under UVA.

In general, humic substances are known to act as photosensitizers that are capable of generating reactive species. However, under irradiation these substances can also be (self)degraded, in a process known as photo-bleaching [41]. In order to determine the effect of the light on the organic matter, a set of tests involving indirect measurements of photo-activity and the aromaticity indices reviewed in [42] was obtained (as in [43]) by recording their spectra during solar irradiation. A summary of the indices and the corresponding results can be found in Table 1.

Under solar light exposure conditions, the changes in these parameters were limited but observable, with the indices tending to increase. The spectra of the humic substances exhibited considerable change throughout the entire spectral range (Figs. S1–4). The

Table 1
Summary of photo-chemical and aromaticity indices changes during solar exposure.

Parameter/Time (min)	0	30	60	120	180
HA5					
E_2/E_3 (A_{254}/A_{365})	2.32	2.29	2.29	2.27	2.31
E_4/E_6 (A_{465}/A_{665})	3.15	2.95	2.91	3.00	2.78
ε_{280} (A_{280}/C (L mg^{-1} cm^{-1}))	0.03	0.03	0.03	0.03	0.03
SUVA (A_{254}/TOC mg C L^{-1})	4.11	4.25	4.46	4.76	5.01
Slope ratio S_R ($s_{(275–295)}/s_{(350–450)}$)	0.70	0.72	0.73	0.77	0.96
HA16					
E_2/E_3 (A_{254}/A_{365})	2.32	2.31	2.33	2.35	2.42
E_4/E_6 (A_{465}/A_{665})	3.50	3.35	3.11	3.29	3.24
ε_{280} (A_{280}/C (L mg^{-1} cm^{-1}))	0.03	0.03	0.03	0.03	0.03
SUVA (A_{254}/TOC mg C L^{-1})	3.95	4.06	4.19	4.43	4.85
Slope ratio S_R ($s_{(275–295)}/s_{(350–450)}$)	0.64	0.68	0.68	0.71	0.89

irradiation consistently increased ε_{280} (Fig. S3), $SUVA_{254}$ (Fig. S4), and S_R (Fig. S5) in the both the HA_5 and HA_{16} samples, while the E_4/E_6 and E_2/E_3 ratios decreased slightly (Figs. S6–7). Del Vecchio et al. proposed a model to interpret the absorption spectra of humic substances: The energy transitions at short wavelengths ($\lambda < 300$ nm) are due to the individual absorptions of the electron donor D (e.g., poly-hydroxylated aromatics, phenols, or indoles) and the electron acceptor A (e.g., quinones) moieties, while the long wavelength absorptions arise from a ground-state interaction between D and A, namely "charge-transfer complexes" [44,45]. Other authors have found that irradiation of humic substances induces changes in their optical properties. For example, when HS are irradiated for short times, a decrease in absorption at longer wavelengths is observed, indicating the destruction of the charge-transfer complexes [41,46]. Hence, this is a possible explanation for the increases in $SUVA_{254}$ and ε_{280} observed in this study, since the destruction of these charge-transfer complexes would enhance the individual absorbance of the donors and acceptors at lower wavelengths.

Additionally, a relationship between the spectral slope and the molecular weight has been reported, with the spectral slope increasing with decreasing molecular weight. The slope ratio (S_R) parameter was measured to determine the photo-oxidation of the organic matter, and in our results, $S_{275–295}$ showed greater variation than the $S_{350–400}$ region. Table 1 shows that the S_R increased with irradiation time in both HA_5 and HA_{16}. Other authors also have found that S_R increases with photo-bleaching [41,46,47]. The ratio E_2/E_3 has been established as a relative measure of the contribution of charge-transfer complexes [48]. The donor and acceptor species absorb at 254 nm while the charge-transfer complexes typically show absorbance at 365 nm. Hence a low E_2/E_3 ratio indicates a greater contribution from the charge transfer complexes [47]. The increase in the E_2/E_3 ratio is related to the relatively lower degradation of the aromatic fractions compared to the charge transfer complexes under irradiation. Finally, the ratio E_4/E_6 has been reported to be inversely related to chromophoric DOM (CDOM) aromaticity [49]. As such, the decrease in the E_4/E_6 ratio obtained under irradiation is consistent with the destruction of the charge-transfer complexes and the availability of absorbing aromatic compounds (D and A). The percent change in the parameters for HA_5 and HA_{16} was similar (slightly higher for HA_{16}, 1–5%), which might affect bacterial inactivation as shown in Fig. 4. The modification of the long wavelength indices also explains the differences observed under visible light.

3.3. Effect of Fe and Cu content in humic acids on the inactivation of E. coli by $h\nu/H_2O_2$

The second step in the photo-Fenton (Fig. 5) process is the addition of H_2O_2 to HA; typical concentrations of H_2O_2 for drinking water treatment processes were used [50]. In principle, the system is heavily modified in the presence of H_2O_2, as triplet states and the singlet oxygen in the *hv*-only system cause far less inactivation than in the combined $h\nu/H_2O_2$ system. More specifically, the shortest inactivation time without added H_2O_2 was 300 min, while in the $h\nu/H_2O_2$ system the time was halved, even in the absence of HA. Hence, we will consider the effect of *hv* as the baseline degradation, but we will not further investigate its importance. The addition of small amounts of HA_{16} increased the inactivation efficiency, but an inhibitory effect on the inactivation process was observed as the concentration of HA_{16} was increased from 0.1 mg/L to 1 mg/L (Fig. 5). These results suggest that HA played a scavenger role during the process, which was unexpected considering its metal content. Therefore, assays were conducted using increased amounts of H_2O_2. Fig. 5B shows the results of bacterial inactivation in the absence and presence of the three different humic acids using the optimum concentration determined from Fig. 5A (0.1 mg/L) and 10 or 15 mg/L H_2O_2.

The addition of H_2O_2 in the dark did not cause inactivation of the bacteria, indicating that although H_2O_2 is considered an oxidant, at the

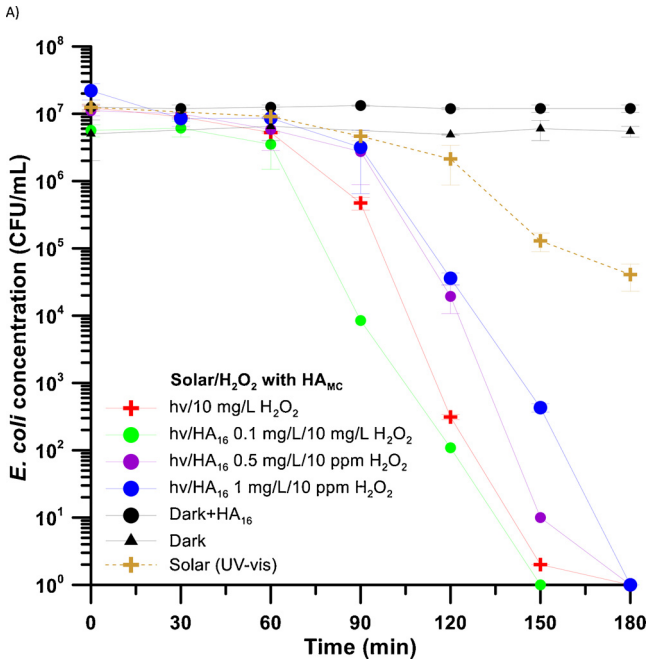

Fig. 5. Photo-inactivation ($h\nu > 290$ nm) of an *E. coli* suspension in Milli-Q water (pH 6–6.5). **A)** Photo-inactivation using different quantities of HA_{16} and 10 mg/L H_2O_2: (●) $h\nu/H_2O_2/HA_{16}$ 0.1 mg/L, (●) $h\nu/H_2O_2/HA_{16}$ 0.5 mg/L, (●) $h\nu/H_2O_2/HA_{16}$ 1 mg/L, (✚) $h\nu/H_2O_2$, and dark and control experiments. **B)** Photo-inactivation using 0.1 mg/L of the different humic acids and 10 mg/L H_2O_2: (●) HA_1; (●) HA_5; (●) HA_{16}, and dark and control experiments: (●) only HA_5; (-▲-) only H_2O_2; (■) $h\nu/H_2O_2/HA_{16}$ (15 mg/L H_2O_2 and 0.1 mg/L HA_{16}); (✚) HA_{16}/H_2O_2 15 mg/L (without HA).

studied concentrations, its effect is negligible. The inactivation by $h\nu/H_2O_2$ in the absence of HA showed a significant improvement, requiring approximately 155 min for total inactivation. Moreover, hydrogen peroxide can penetrate into cells and under illumination, high intracellular H_2O_2 concentration increases the possibility of $HO^{\bullet}$ generation via the Fenton reaction with intracellular iron. H_2O_2 can also cause the oxidation of iron sulfur clusters, releasing Fe^{3+} [51]. This is the most probable explanation for the independence of the amount of bacterial damage on the hydrogen peroxide concentration; both concentrations of hydrogen peroxide used (10 and 15 mg/L) were lethal to the bacteria after 150 min, since 10 mg/L was enough to cause this intracellular imbalance.

More interesting is the order of efficiency in the presence of the different HA samples, compared to that observed in the solar only experiments. In the presence of H_2O_2, the relative photo-inactivation trend was the opposite of that observed in the absence of H_2O_2, i.e., $HA_{16} > HA_5 > HA_1$. Additionally, only HA_{16} showed an enhancement effect; the inactivation of *E. coli* was achieved in 150 min in the presence of 10 mg/L of H_2O_2, while the addition of 15 mg/L of H_2O_2 reduced this to 120 min. In contrast, in the presence of HA_5 and HA_1, a decrease in *E. coli* inactivation was observed. A possible explanation for this phenomenon lies in the composition of the different HAs.

Since the ESD used for the characterization of the minerals is a semi-quantitative technique, ICP-MS analysis was carried out during the irradiation tests to assess the soluble Fe and Cu content that was generated in the samples (Table 2). As can be seen in both samples, both metals exist in the solution, but for Fe, a decreasing tendency due to the operational pH and the induced precipitation was found. A thermodynamic analysis based on stability constants was performed using the software MEDUSA. The stability constants were calculated using this software. The species distribution diagrams for Cu and Fe taking into account the pH of the system and the possibility of oxidation of Fe^{2+} to Fe^{3+} are shown in Fig. S8 (Supporting material). From these diagrams,

Table 2
ICP-MS measurements for the soluble fraction of Fe and Cu during solar irradiation of HA_5 and HA_{16}.

Humic Acid	min	ppb	
	Time	Fe	Cu
HA_5	0	2.52	3.68
	60	2.14	4
	120	2.02	4.7
	180	2.38	4.62
HA_{16}	0	2.26	2.83
	60	1.78	4.57
	120	1.06	4.38
	180	0.38	2.73

the lower fraction of Fe^{2+} in the solution despite the higher Fe content can be explained. At the pH of the ICP-MS analysis (6.5) the amount of soluble Fe^{2+} species was low, while the concentration of Cu^{2+} was at a maximum. Based on the amounts of Cu and Fe leached during the bacterial inactivation process, the enhancement observed in the HA-containing $h\nu/H_2O_2$ system was due to the soluble fraction of mineral matter in this sample (Tables 2 and S1), which generated photo-Fenton and photo-Fenton-like processes.

Furthermore, iron, copper, and humic substances have been proposed to form stable metal-HS complexes in solution [52], which can efficiently facilitate the generation of ROS, by decreasing the redox potential and facilitating the Fenton process. This effect has been described by other authors [53,54]. Cu and Fe can bind to S, N, COO^-, and other electron donating groups on the bacteria cell wall, as well as permeating through the cell membrane in ppb amounts to reach the cytoplasm, leading to bacterial inactivation. These metals have been reported to undergo photo-reduction in the UV–vis region when bound with organic components [55,56]. This process may enhance bacterial inactivation through ligand-to-metal charge transfer (LMCT).

$$\text{LMCT for copper: } (Cu^{+2} - HA) + h\nu \rightarrow Cu^{+} + HA_{ox}^{+} \quad (21)$$

Also, in addition to the HAs, the bacterial surface has been reported to act as a sacrificial electron donor, leading to cell wall damage [39].

Another important point to note in Fig. 5B is that HA_5 and HA_1 were less efficient than $h\nu/H_2O_2$. This decrease in efficiency can be explained by the $HO^{\bullet}$ scavenging action of the humic substances (Eq. 22). $HO^{\bullet}$ attacks the organic HA molecules, leading to a decrease in the amount of ROS available to attack the bacterial cells. Therefore, when HA is not present in solution, more hydroxyl radicals are available to attack *E. coli* cells; however, when the mineral content is high, the increased $HO^{\bullet}$ production may compensate for this effect. The competition between organic matter degradation and microbial inactivation during photo-Fenton reaction has been previously demonstrated. In fact, several authors have observed clear competition between an organic compound (resorcinol) and a model microorganism (*Enterococcus faecalis*) for oxidant species, mainly hydroxyl radicals generated during the photo-Fenton reaction [32,57].

$$HA + HO^{\bullet} \rightarrow HA_{ox}^{+} + HO^{-} \quad (22)$$

As a final proof of concept for photo-Fenton participation in bacterial inactivation with only the addition of H_2O_2, the H_2O_2 consumption was measured in the presence and absence of HA. As shown in Fig. 6, the greatest H_2O_2 consumption was observed in the presence of HA_{16}, demonstrating the reaction between H_2O_2 and the iron and copper in the sample. Additionally, although the H_2O_2 consumption was higher in the presence of HA_1 and HA_5 than without HA, the bacterial inactivation was lower; hence, it was hypothesized that HA is simultaneously being degraded. In the next section, we will assess this hypothesis using more intense photo-Fenton conditions.

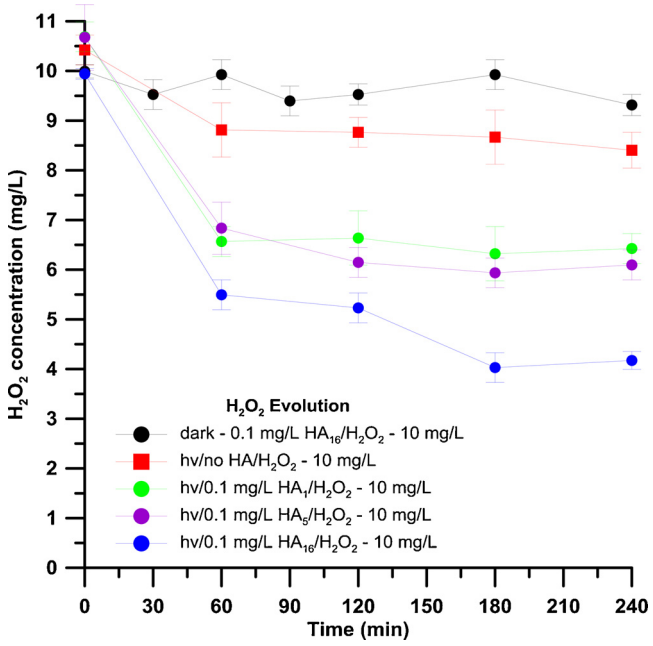

Fig. 6. H_2O_2 consumption during photo-inactivation ($h\nu > 290$) of an *E. coli* suspension in Milli-Q water (pH 6–6.5) containing 0.1 mg/L of different humic acids and 10 mg/L H_2O_2. (■) $h\nu$ only (without HA); (●) HA_1; (●) HA_5; (●) HA_{16} and (●) dark control.

3.4. Effect of the humic acid isolates on E. coli inactivation by the photo-Fenton reaction

In the final part of the investigation, the addition of both H_2O_2 and Fe (15 and 1 mg/L, respectively) was carried out to enhance the photo-Fenton process, and to support or disprove the hypotheses described in the previous section based on the results of the $h\nu$ and $h\nu/H_2O_2$ experiments. Namely, the enhancement resulting from HA addition, the scavenging of oxidants, the complexation and subsequent LMCT, and the fate of the HAs were studied. Fig. 7 shows the inactivation of *E. coli*

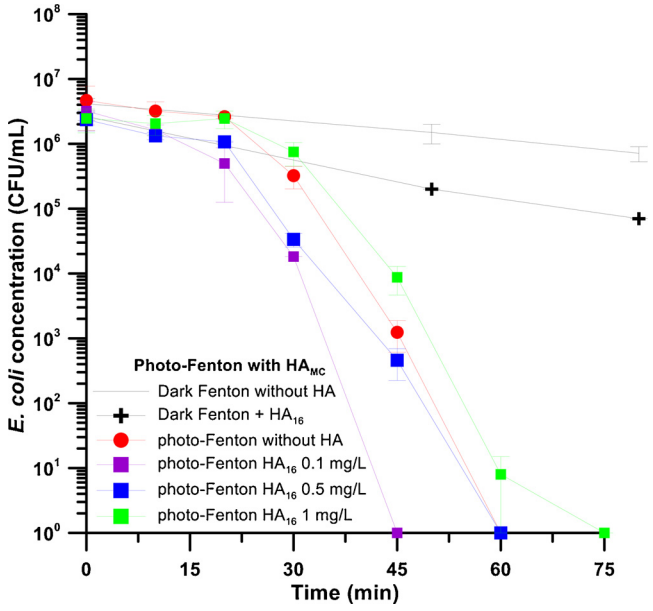

Fig. 7. Fenton and photo-Fenton inactivation of an *E. coli* suspension in Milli-Q water (pH 6–6.5) with 1 mg/L of Fe^{2+} and 15 mg/L of H_2O_2 and different quantities of HA_{16}. (●) without HA; (■) 1 mg/L; (■) 0.5 mg/L; and (■) 0.1 mg/L; and dark controls: (--) Fenton; (✚) Fenton + HA.

using the classical Fenton and photo-Fenton systems in the absence and presence of various concentrations of HA_{16}.

The blank process (dark Fenton) interestingly showed 1-logU higher inactivation when HA_{16} was added. Enhanced inactivation *E. coli* was observed for the Fenton reaction in the presence of HA compared to the classical Fenton reaction after 80 min of reaction time. The formation of stable HA-iron complexes resulted in the iron remaining in solution at this pH for a longer time, leading to more effective bacterial inactivation. Additionally, the inactivation of *E. coli* was significantly increased under light. In these systems, $HO^{\bullet}$ and ROS generation inside or close to the cell may occur simultaneously. More specifically, the presence of extracellular H_2O_2 was analyzed previously, but the further addition of iron may enhance the generation of extracellular $HO^{\bullet}$ and other ROS that can attack the bacterial cells from the outside, initiating lipid peroxidation chains and enhanced membrane damage. Since the photo-Fenton inactivation mechanism has been recently reviewed [5], here we will focus only on details specific to these HAs.

Although the presence of organic matter could be seen as a problem, as it could consume $HO^{\bullet}$ or attenuate the active light, the results showed increased inactivation in the presence of HA (Fig. 7). Humic substances are known to contain a high density of carboxylate functional groups that complex with iron [58]. HA_{16} improved the solubility of iron during the photo-Fenton process, and its degradation intermediates formed complexes with iron, which are photoactive at neutral pH. In particular, Fe^{3+}-organo complexes are generally stable at near neutral pH and show higher light absorption in the solar light range than hydroxyl complexes [59,60].

In order to confirm the formation of Fe-complexes, a UV–vis titration in which iron was added to HA_5 and HA_{16} solutions (50 mg/L) was carried out (Supporting information Figs. S9 and S10, respectively). The absorbance at 500 nm was measured (Supporting information Fig. S11). The titration results clearly showed the formation of complexes; a saturation point was observed for the solution (2.125 mL) at 171 mg of iron (II). Thus, 0.1 mg of HA is able to complex 171 mg of iron (II). In both samples, an inversion of the absorbance was clearly observed at 398 nm. This is known as an isosbestic point, and indicates that there are two species in equilibrium with the same absorptivity coefficient. One of these species corresponds to the humic acid, and the other one is most probably the complex of humic acid and iron.

Furthermore, the enhancement in the *E. coli* inactivation was a function of the HA concentration. Considering that rate constant of the reaction of $HO^{\bullet}$ with humic substances is on the order of 3×10^4 mg/L of DOC/s [61], the humic substances are in competition with the microorganisms in the reaction with $HO^{\bullet}$ and with the reactive species generated in the photo-Fenton process [57]. In order to assess the theory that the organic matter acts as a $HO^{\bullet}$ scavenger, the absorption spectra and the peroxide consumption were measured during the photo-Fenton process. Figs. S12 and S13 (Supporting material) show the results for HA_5 and HA_{16}, respectively.

The spectrophotometric investigation showed that the consumption of hydrogen peroxide was greater when HA_{16} was used, and that greater changes in the absorbance spectrum were observed for the HA_{16} sample than the HA_5 sample. This is a clear indication of an additional contribution from the mineral matter contained in HA_{16}, as hypothesized in the previous section. The spectra show that the absorbance was greatly decreased during the photo-Fenton reaction, indicating greater degradation of the humic acids during this process. The decrease in absorbance was more evident for HA_{16}, and in some cases different trends were observed between HA_{16} and HA_5.

The changes in the HA spectral indices observed during the photo-Fenton process were more significant than those that occurred during the solar irradiation process. The same photo-activity and aromaticity indices (i.e., ε_{280}, $SUVA_{254}$, S_R, E_2/E_3, and E_4/E_6) were determined for the photo-Fenton process, and the results are summarized in Table 3. The decrease in these indices was proportional to the mineral content of the HA. We suggest that the oxidative action of the photo-Fenton process induces considerable changes in the nature of the HA. During the first 30 min, the A–D charge-transfer complexes were destroyed, causing an increase in the absorbance at low wavelengths, which is consistent with the parameters measured. However, after this time, the destruction of the chromophores became more effective. The decrease in absorption and in the parameters ε_{280}, $SUVA_{254}$, and E_2/E_3 demonstrated the degradation of the chromophores. Thus, the addition of HA initially enhanced the photo-Fenton process, but over the course of the experiments, the self-degradation of HA proceeded in a more effective manner than under solar light alone. Although the indices followed similar trends, the HA_{16} spectrum was less affected in the visible region (E_4/E_6), showed a lower $SUVA_{254}$ increase, and a higher decrease in S_R. These measurements indicated that both HA_5 and HA_{16} were degraded, but in a different manner depending on the metal content That is, in HA_{16}, the visible region was less affected and the UV absorbance was more affected, leading to the destruction of high-energy bonds. Overall, the global impact of HA on solar disinfection kinetics is a combination of both beneficial and antagonistic action modes. HA enhances ROS production due to the ROS generated by the illumination of the NOM, i.e., singlet oxygen, H_2O_2, and triplet states of HA. On the other hand, HA decreases the inactivation rates by quenching the generated ROS, including hydroxyl radicals, when additional H_2O_2 is introduced, and its photo-screening properties lead to light absorption without photochemical activity for disinfection.

Table 3
Summary of photo-chemical and aromaticity indices alterations during the photo-Fenton process.

Parameter/Time (min)	0	30	60	180
HA_5				
E_2/E_3 (A_{254}/A_{365})	2.31	2.35	2.36	2.36
E_4/E_6 (A_{465}/A_{665})	2.88	2.92	2.79	2.76
ε_{280} (A_{280}/C ($L\,mg^{-1}\,cm^{-1}$))	0.03	0.03	0.03	0.03
SUVA (A_{254}/TOC $mg\,C\,L^{-1}$)	4.44	4.75	5.03	6.12
Slope ratio S_R ($s_{(275–295)}/s_{(350–450)}$)	0.70	0.58	0.55	0.55
HA_{16}				
E_2/E_3 (A_{254}/A_{365})	2.30	2.30	2.27	2.25
E_4/E_6 (A_{465}/A_{665})	2.91	2.95	3.00	2.88
ε_{280} (A_{280}/C ($L\,mg^{-1}\,cm^{-1}$))	0.03	0.03	0.03	0.02
SUVA (A_{254}/TOC $mg\,C\,L^{-1}$)	4.46	4.61	4.77	5.11
Slope ratio S_R ($s_{(275–295)}/s_{(350–450)}$)	0.65	0.49	0.45	0.40

4. Conclusions

In this work, the use of naturally extracted humic acids to enhance solar-based disinfection methods was investigated. HAs containing metals (Fe, Cu) were evaluated in pure SODIS, with added H_2O_2, and with the simultaneous addition of Fe and H_2O_2 to induce the photo-Fenton process. The main differences in these processes lie in the mechanisms by which the process is enhanced, which in turn depend on whether H_2O_2 and/or Fe are added. The SODIS enhancement is related to the organic matter content; the enhancement when H_2O_2 is added is due to the induction of a photo-Fenton process by the natural metal content of the HA; and the enhancement observed with Fe and H_2O_2 is the result of the complexation of Fe by the HAs.

More specifically, the SODIS performance was only enhanced when demineralized HA samples were used. The higher C content was indirectly correlated with the photo-activity, as shown by the spectrophotometric analyses. Both the excited triplet states of the organic matter ($^3HA^*$) and singlet oxygen were found to be responsible for the inactivation of *E. coli*. The HAs with higher mineral contents were not beneficial, although they presented higher photo-activity in the visible region and similar UV light absorption. This is most likely due to the higher percentage of ketonic and quinonic compounds in the low mineral samples. The relative order of disinfection efficiency was $HA_1 > HA_5 > HA_{16}$.

As expected, the addition of H_2O_2 enhanced the inactivation of microorganisms in the absence of HAs. However, the driving force of the inactivation was suggested to be photo-Fenton and photo-Fenton like processes driven by Fe and Cu, respectively. The destruction of the HA structure led to the release of metals in solution, creating oxidative conditions. HAs with greater C content demonstrated lower activity than in the *hv*/H_2O_2-only conditions, and high (15 mg/L) concentrations of H_2O_2 better exploited the metal-driven photo-Fenton efficiency. The consumption of H_2O_2 verified that the photo-Fenton process took place.

Moreover, the simultaneous addition of Fe and H_2O_2 enhanced the photo-Fenton process, but only at low HA concentrations that avoided high rates of radical self-scavenging. The HAs were shown to form stable, photoactive complexes in the presence of iron. As such, the bactericidal LMCT activity was enhanced, and less Fe precipitation occurred during the photo-Fenton cycle, leading to greater Fe activity. The spectrophotometric analyses revealed the simultaneous degradation of the HAs, mainly in the visible region. The HAs played the roles of sacrificial ligand and fuel for the photo-Fenton process.

In particular, the evolution of $SUVA_{254}$ and S_R values during treatment revealed that the SODIS process only affected the highly reductive NOM content (e.g., ketones), which are sensitive to the weaker ROS (compared to $HO^{\bullet}$), such as $^3HA^*$ and $^1O_2$ that are generated during the illumination of HA in the absence of (added) H_2O_2 and Fe. On the other hand, the photo-Fenton process affects the less reductive moieties of NOM, such as aromatic rings (i.e., benzene), which are only sensitive to highly oxidative ROS, such as $HO^{\bullet}$. As a result, the Fe-enhanced process effectively removes bacteria and also reduces the amount of organic matter in the bulk. This effect can be crucial when removal of both DOM and microorganisms is sought.

Acknowledgements

The authors gratefully acknowledge the Universidad de Antioquia (UdeA) for funding the research. Jazmin Porras would like to acknowledge the Colombian Administrative Department of Science, Technology and Innovation (COLCIENCIAS) for her Ph.D. Stefanos Giannakis and Cesar Pulgarin would like to acknowledge the European project WATERSPOUTT H2020-Water-5c-2015 (GA 688928) for the financial support.

Appendix A. Supplementary data

Supplementary material related to this article can be found, in the online version, at doi:https://doi.org/10.1016/j.apcatb.2018.04.062.

References

[1] K.G. McGuigan, R.M. Conroy, H.J. Mosler, M. du Preez, E. Ubomba-Jaswa, P. Fernandez-Ibanez, J. Hazard. Mater. 235–236 (2012) 29–46.
[2] J. Ndounla, D. Spuhler, S. Kenfack, J. Wéthé, C. Pulgarin, Appl. Catal. B: Environ. 129 (2013) 309–317.
[3] S. Giannakis, Environ. Sci. Pollut. Res. (2017) 1–17, http://dx.doi.org/10.1007/s11356-017-0926-x.
[4] R.G. Zepp, B.C. Faust, J. Holgné, Environ. Sci. Technol. 26 (1992) 313–319.
[5] S. Giannakis, M.I. Polo López, D. Spuhler, J.A. Sánchez Pérez, P. Fernández Ibáñez, C. Pulgarin, Appl. Catal. B: Environ. 199 (2016) 199–223.
[6] A. Paul, S. Hackbarth, R.D. Vogt, B. Röder, B.K. Burnison, C.E.W. Steinberg, Photochem. Photobiol. Sci. 3 (2004) 273–280.
[7] C. Richard, S. Canonica, Aquatic phototransformation of organic contaminants induced by coloured dissolved natural organic matter, in: O. Hutzinger (Ed.), The Handbook of Environmental Chemistry, vol. 2, Springer, 2005, pp. 299–323 Part M.
[8] S.L.H. Sandvik, P. Bilski, J.D. Pakulski, C.F. Chignell, R.B. Coffin, Mar. Chem. 69 (2000) 139–152.
[9] M.J. Mattle, D. Vione, T. Kohn, Environ. Sci. Technol. 49 (2014) 334–342.
[10] S. Bahnmüller, U. von Gunten, S. Canonica, Water Res. 57 (2014) 183.
[11] D. Vione, F. Merlo, V. Maurino, C. Minero, Environ. Chem. Lett. 2 (2004) 129–133.
[12] T. Kohn, K.L. Nelson, Environ. Sci. Technol. 41 (2007) 192–197.
[13] R.H. Reed, Adv. Appl. Microbiol. 54 (2004) 333–365.
[14] D. Vione, M. Minella, V. Maurino, C. Minero, Chem. -Eur. J. 20 (2014) 10590.
[15] J. Chen, B. Gu, E.J. LeBoeuf, H. Pan, S. Dai, Chemom. Intell. Lab. Syst. 48 (2002) 59–68.
[16] Y. Chen, C. Hu, X. Hu, J. Qu, Environ. Sci. Technol. 43 (2009) 2760–2765.
[17] R.M. Cory, D.M. McKnight, Environ. Sci. Technol. 39 (2005) 8142–8149.
[18] Z. Yang, A. Kappler, J. Jiang, Environ. Sci. Technol. 50 (2016) 12105–12113.
[19] R.M. Cory, D.M. McKnight, Environ. Sci. Technol. 39 (2005) 8142.
[20] S.A. Green, N.V. Blough, Limnol. Oceanogr. 39 (1994) 1903.
[21] J.A. Korak, A.D. Dotson, R.S. Summers, F.L. Rosario-Ortiz, Water Res. 49 (2014) 327.
[22] U.J. Wünsch, K.R. Murphy, C.A. Stedmon, Front. Mar. Sci. 2 (2015).
[23] Y. Chen, L. Liu, J. Su, J. Liang, B. Wu, J. Zuo, Y. Zuo, Chemom. Intell. Lab. Syst. 187 (2017) 261–267.
[24] R.R. Chowdhury, P.A. Charpentier, M.B. Ray, J. Photochem. Photobiol. A Chem. 219 (2011) 67–75.
[25] J. Porras, J.J. Fernandez, R.A. Torres-Palma, C. Richard, Environ. Sci. Technol. 48 (2014) 2218–2225.
[26] J. Porras, C. Bedoya, J. Silva-Agredo, A. Santamaría, J.J. Fernández, R.A. Torres-Palma, Water Res. 94 (2016) 1–9.
[27] A. Moncayo-Lasso, J. Sanabria, C. Pulgarin, N. Benitez, Chemom. Intell. Lab. Syst. 77 (2009) 296–300.
[28] D. Spuhler, J.A. Rengifo-Herrera, C. Pulgarin, Appl. Catal. B Environ. 96 (2010) 126–141.
[29] M. Drosos, M. Ren, F.H. Frimmel, Appl. Catal. B: Environ. 165 (2015) 328–334.
[30] C.S. Uyguner-Demirel, N.C. Birben, M. Bekbolet, Catal. Today 284 (2017) 202–214.
[31] E. Ortega-Gómez, B.E. García, M.B. Martín, P.F. Ibáñez, J.S. Pérez, Water Res. 63 (2014) 316–324.
[32] A. Moncayo-Lasso, L.E. Mora-Arismendi, J.A. Rengifo-Herrera, J. Sanabria, N. Benítez, C. Pulgarin, Photochem. Photobiol. Sci. 11 (2012) 821–827.
[33] S. Giannakis, S. Liu, A. Carratalà, S. Rtimi, M. Bensimon, C. Pulgarin, Appl. Catal. B: Environ. 204 (2017) 156–166.
[34] S. Giannakis, S. Liu, A. Carratalà, S. Rtimi, M. Talebi Amiri, M. Bensimon, C. Pulgarin, J. Hazard. Mater. 339 (2017) 223–231.
[35] E.E. Daugherty, B. Gilbert, P.S. Nico, T. Borch, Environ. Sci. Technol. 51 (2017) 11096–11104.
[36] B.M. Voelker, F.M.M. Morel, B. Sulzberger, Environ. Sci. Technol. 31 (1997) 1004–1011.
[37] S. Giannakis, E. Darakas, A. Escalas-Cañellas, C. Pulgarin, Chem. Eng. J. 281 (2015) 588–598.
[38] L. Carlos, D.O. Mártire, M.C. Gonzalez, J. Gomis, A. Bernabeu, A.M. Amat, A. Arques, Water Res. 46 (2012) 4732–4740.
[39] D. Spuhler, J. Andrés Rengifo-Herrera, C. Pulgarin, Appl. Catal. B: Environ. 96 (2010) 126–141.
[40] M.A.J. Rodgers, P.T. Snowden, J. Am. Chem. Soc. 104 (1982) 5541.
[41] R. Del Vecchio, N.V. Blough, Mar. Chem. 78 (2002) 231–253.
[42] C. Uyguner-Demirel, M. Bekbolet, Chemom. Intell. Lab. Syst. 84 (2011) 1009–1031.
[43] S. Giannakis, M. Voumard, D. Grandjean, A. Magnet, L.F. De Alencastro, C. Pulgarin, Water Res. 102 (2016) 505–515.
[44] E.S. Boyle, N. Guerriero, A. Thiallet, R.D. Vecchio, N.V. Blough, Environ. Sci. Technol. 43 (2009) 2262.
[45] R. Del Vecchio, N.V. Blough, Environ. Sci. Technol. 38 (2004) 3885.
[46] C.M. Sharpless, N.V. Blough, Environ. Sci.: Processes Impacts 16 (2014) 654.
[47] J.R. Helms, A. Stubbins, J.D. Ritchie, E.C. Minor, D.J. Kieber, K. Mopper, Limnol. Oceanogr. 53 (2008) 955–969.
[48] R.M. Dalrymple, A.K. Carfagno, C.M. Sharpless, Environ. Sci. Technol. 44 (2010) 5824–5829.
[49] C.S. Uyguner, M. Bekbolet, Dermatol. Surg. 176 (2005) 47–55.
[50] S. Giannakis, M.I. Polo López, D. Spuhler, J.A. Sánchez Pérez, P. Fernández Ibáñez, C. Pulgarin, Appl. Catal. B: Environ. 198 (2016) 431–446.
[51] J.A. Imlay, Ann. Rev. Microbiol. 57 (2003) 395–418.
[52] J.J. Pignatello, E. Oliveros, A. MacKay, Crit. Rev. Environ. Sci. Technol. 36 (2006) 1–84.
[53] E. Rentz, J. Nutr. Environ. Med. 13 (2003) 109–118.
[54] L. Suárez, Z. Wei, H. Teixidó, R. Sanjinés, M. Bensimon, C. Pulgarín, J. Kiwi, J. Environ. Chem. Eng. 5 (2017) 310–318.
[55] J. Kim, I. Metcalfe, Chemosphere 69 (2007) 689–696.
[56] A.N. Pham, G. Xing, C.J. Miller, T.D. Waite, J. Catal. 301 (2013) 54–64.
[57] E. Ortega-Gómez, M.M. Ballesteros Martín, B. Esteban García, J.A. Sánchez Pérez, P. Fernández Ibáñez, B. Applied Catalysis, Environmental 148–149 (2014) 484–489.
[58] R.C. Averett, J. Leenheer, D.M. McKnight, K. Thorn, Humic Substances in the Suwannee River, Georgia; Interactions, Properties, and Proposed Structures, USGPO; US Geological Survey, Map Distribution, (1994).
[59] A. Georgi, A. Schierz, U. Trommler, C.P. Horwitz, T.J. Collins, F.D. Kopinke, Appl. Catal. B: Environ. 72 (2007) 26–36.
[60] B.M. Voelker, B. Sulzberger, Environ. Sci. Technol. 30 (1996) 1106–1114.
[61] J. Hoigné, B.C. Faust, W.R. Haag, F.E. Scully, R.G. Zepp, Adv. Chem. Ser. 219 (1989) 363.
[62] Y. Chen, H. Li, Z. Wang, H. Li, T. Tao, Y. Zuo, Water Res. 46 (2012) 2965–2972.
[63] S. Giannakis, A.I. Merino Gamo, E. Darakas, A. Escalas-Cañellas, C. Pulgarin, Chem. Eng. J. 253 (2014) 366–376.
[64] S. Giannakis, C. Ruales-Lonfat, S. Rtimi, S. Thabet, P. Cotton, C. Pulgarin, Appl. Catal. B: Environ. 185 (2016) 150–162.
[65] M. Mangayayam, J. Kiwi, S. Giannakis, C. Pulgarin, I. Zivkovic, A. Magrez, S. Rtimi, Appl. Catal. B: Environ. 202 (2017) 438–445.